



# Effects of non-uniform wall properties on stress distribution in an abdominal aortic aneurysm, considering nonlinear constitutive equations

G.R. Zendhebudi\*

*Department of Mechanical Engineering, Yasouj University, Yasouj, Iran.*

Received 19 October 2012; received in revised form 25 August 2013; accepted 28 October 2013

## KEYWORDS

Finite element method;  
 Aneurysm rupture;  
 Aneurismal wall;  
 Thick-wall theory;  
 Blood pressure;  
 Abdominal aortic aneurysm;  
 Non-linear constitutive equation.

**Abstract.** In this study, stress distribution in the aneurismal wall of the abdominal aortic is addressed. Full equilibrium equations derived from the thick-wall theory are solved using the well-known Finite Element Method (FEM). Nine-node quadratic rectangular plane elements are employed for the spatial discretization of the computational domain. Non-linear constitutive equations and non-uniform wall properties are taken into consideration. The results of this investigation show that in addition to the aneurysm size, some other factors may significantly affect stress distribution in aneurismal wall. Factors such as wall thickness, blood pressure and longitudinal tension have been identified for both uniform and non-uniform wall properties. Having numerically simulated different cases, it is demonstrated that longitudinal stress is the maximum stress in the wall, and it is not significantly affected by the uniformity of wall stiffness.

© 2014 Sharif University of Technology. All rights reserved.

## 1. Introduction

An aneurysm is an abnormal dilatation of a portion of an artery due to a weakening in the vessel wall which may happen either congenitally or by disease. Aneurysm is a major threat to rupture, if left untreated. There are several types of aneurysm, such as Abdominal Aortic Aneurysm (AAA), brain (cerebral) aneurysm, and Thoracic Aortic Aneurysm (TAA) [1]. Each type of aneurysm may be further subdivided into fusiform, saccular, or dissecting. The fusiform aneurysm is axisymmetric; the saccular has the shape of a sac, and the dissecting aneurysm results from the diffusion of the blood between the separated layers of the arterial wall.

In the present work, the fusiform aneurysm is considered. The axisymmetric stress distributions are examined to evaluate the effect of factors such as aneurysm radius, blood pressure and the longitudi-

nal tension on the maximum stress generated in the aneurysm wall with both uniform and non-uniform stiffness.

It is necessary to point out that stiffness non-uniformity is caused by the aneurysm. This non-uniformity along the longitudinal direction is more important than the stiffness non-uniformity in the radial direction, i.e. across the thickness. In the radial direction, a normal artery has three layers (intima, media and adventitia), although the aneurysm wall has only two layers, because of an abnormal loss or absence of the muscular layer. From two remaining layers, the media is the most important for determining the biomechanical properties of the artery wall. It contains smooth muscle cells, which are oriented circumferentially and have an important influence on arterial stiffness.

A common practice to repair the aneurysm is surgical resection. However, since this practice involves major surgery with a high mortality rate [2,3], it is prudent to repair the aneurysm only when there

\*. E-mail address: zendhebudi@yu.ac.ir (G.R. Zendhebudi)

is objective evidence that the aneurysm rupture is imminent. To diagnose whether the aneurysm rupture is imminent or not, an appropriate criterion must be applied. Although the aneurysm size is usually used as a criterion, clinicians are aware of the fact that some aneurysms rupture at an unusually small size [4,5]. Therefore, a preferred criterion is the maximum stress generated in the aneurysm wall. To prevent rupturing, the maximum stress should be less than the strength of the wall tissue. In other words, if the maximum stress in the aneurysm wall exceeds the strength of the wall tissue, aneurysm rupture will be imminent.

To compute maximum stress, one has to determine the stress distribution in the wall. To do this, several methods, such as the thick-wall theory, the membrane theory, or the method of taking a simple relationship between the blood pressure and aneurysm diameter, could be used. However, as the thick-wall theory is more complicated and leads to expensive computational costs, some investigators prefer to use simpler methods, such as the membrane theory.

In the present study, the stress distributions are calculated using the thick-wall theory by the well-known FEM. Nine-node quadratic rectangular plane elements are used for grid generation. Solving the full equilibrium equations in the thick-wall theory leads to the most accurate results. The validation tests (Section 4) show that the amount of error is so trivial that the solutions obtained by this method could be used as a reference solution to assess the accuracy of the other theories.

To find the maximum stress in the wall, the material properties of the wall are needed. Many investigators have tried to find these properties. For instance, Vorp et al. [6] presented the effect of aneurysm on the tensile strength and biomechanical behavior of the ascending thoracic aorta. Based on their study, the tensile strength of the aneurysm wall is about 1.2 MPa. No significant difference in strength was observed between circumferential and longitudinal specimens.

Other investigators, such as Inzoli et al. [7], Mower et al. [8], Stringfellow et al. [9], Elger et al. [10], and Vorp et al. [11] used the theory of linear elasticity. In this theory, the elastic modulus is considered a constant value. In the literature, this constant value varies from 1 MPa [12] to 8 MPa [13]. Still others have taken a value between these two. For example, Steiger et al. [14] have taken 2.5 MPa as the elastic modulus. Some other researchers, such as Demiray [15], Kyriacou and Humphrey [16], Shah and Humphrey [17], Hademenos et al. [18], Thubrikar et al. [19], and Vorp et al. [6] used a system of non-linear constitutive equations.

In 2009, Merckx et al. [20] studied the effect of initial stress incorporation on stress distribution in the aneurysmal wall. They concluded that the

initial stress incorporation significantly improves the wall displacement accuracy of finite element analysis. To account for the complex three-dimensional arrangement of collagen, Gasser [21] applied a microfiber model approach. In his model, the constitutive relations for collagen fibers were integrated over the unit sphere, which defined the tissue's macroscopic properties.

In 2012, Gasser et al. [22] studied the spatial orientation of collagen fibers in the abdominal aortic aneurysm wall and its relation to wall mechanics. They used two constitutive models for collagen fibers in order to integrate an identified structural information in a macroscopic AAA wall model. They concluded that the mechanical properties of collagen fibers depend largely on their undulation, which is an important structural parameter.

A constitutive description of the wall, which is crucial for AAA wall stress prediction, was demonstrated by Polzer et al. [23], in 2013. They obtained different results using different models. They recommended that different results should not be mutually compared unless different stress gradients across the wall are taken into account.

## 2. Governing equations

As noted already, in the thick-wall theory, full equilibrium equations are considered. These equations are derived from Newton's second law for a differential element of the wall. This derivation can be found in any textbook of solid mechanics, such as Timoshenko and Goodier [24], or Atkins and Fox [25].

Taking into account the axisymmetry in the geometry of the problem (see Figure 1), one can write the equilibrium equations as follows:

$$\frac{\partial}{\partial z}(r\sigma_z) + \frac{\partial}{\partial r}(r\tau) = 0, \quad (1)$$

$$\frac{\partial}{\partial z}(r\tau) + \frac{\partial}{\partial r}(r\sigma_r) = \sigma_\theta, \quad (2)$$

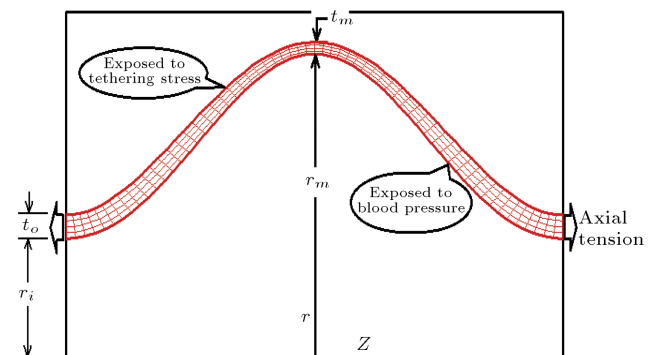


Figure 1. Geometry of the problem and a typical grid used in the finite-element method.

where:

$$\sigma_z = E_{zz} \frac{\partial u}{\partial z} + E_{zr} \frac{\partial v}{\partial r} + E_{z\theta} \frac{v}{r}, \quad (3)$$

$$\sigma_r = E_{rz} \frac{\partial u}{\partial z} + E_{rr} \frac{\partial v}{\partial r} + E_{r\theta} \frac{v}{r}, \quad (4)$$

$$\sigma_\theta = E_{\theta z} \frac{\partial u}{\partial z} + E_{\theta r} \frac{\partial v}{\partial r} + E_{\theta\theta} \frac{v}{r}, \quad (5)$$

$$\tau = G_{zr} \left( \frac{\partial u}{\partial r} + \frac{\partial v}{\partial z} \right), \quad (6)$$

$$E_{zz} = \frac{E_z}{\Delta} \left( 1 - \frac{E_\theta v_r^2}{E_r} \right), \quad (7)$$

$$E_{rr} = \frac{E_r}{\Delta} \left( 1 - \frac{E_z v_\theta^2}{E_\theta} \right), \quad (8)$$

$$E_{\theta\theta} = \frac{E_\theta}{\Delta} \left( 1 - \frac{E_r v_z^2}{E_z} \right), \quad (9)$$

$$E_{zr} = E_{rz} = \frac{1}{\Delta} (\nu_z E_r + \nu_r \nu_\theta E_z), \quad (10)$$

$$E_{z\theta} = E_{\theta z} = \frac{1}{\Delta} (\nu_\theta E_z + \nu_r \nu_z E_\theta), \quad (11)$$

$$E_{\theta r} = E_{r\theta} = \frac{1}{\Delta} (\nu_r E_\theta + \nu_z \nu_\theta E_r), \quad (12)$$

$$\Delta = 1 - \nu_z^2 \frac{E_r}{E_z} - \nu_r^2 \frac{E_z}{E_r} - \nu_\theta^2 \frac{E_z}{E_\theta} - 2\nu_z \nu_r \nu_\theta, \quad (13)$$

$$E_z = [2\alpha_z + 4\beta_z(\lambda_z^2 + 2\lambda_z^{-1} - 3)] (\lambda_z + 1 + \lambda_z^{-1}), \quad (14)$$

$$E_r = [2\alpha_r + 4\beta_r(\lambda_r^2 + 2\lambda_r^{-1} - 3)] (\lambda_r + 1 + \lambda_r^{-1}), \quad (15)$$

$$E_\theta = [2\alpha_\theta + 4\beta_\theta(\lambda_\theta^2 + 2\lambda_\theta^{-1} - 3)] (\lambda_\theta + 1 + \lambda_\theta^{-1}). \quad (16)$$

In Eqs. (3) to (16),  $u$  and  $v$  are displacements in directions  $z$  and  $r$ , respectively.  $\lambda$  is the stretch ratio, and  $\alpha$  and  $\beta$  are non-linear model parameters [6]. As an aneurismal wall is stiffer than a non-aneurismal wall and the stiffness changes continuously along the axis, the following equation is used to consider these changes:

$$E = \frac{E_0}{1 + c \sin^2\left(\frac{\pi z}{2z_m}\right)}, \quad (17)$$

where  $z$  is the distance from the aneurysm center,  $z_m$  is half of the aneurysm length,  $E_0$  is the elastic modulus at the aneurysm center, and  $c$  is the ratio of the aneurismal stiffness to the non-aneurismal stiffness, and depends on the direction. According to Ref. [6],  $c$  is equal to about 0.72 and 0.44 for longitudinal and circumferential directions, respectively.

### 3. Finite-element analysis

In this study, in order to solve the equilibrium equations obtained from the thick-wall theory, the well-known Finite-Element Method (FEM) is employed. In this method, the domain of the problem, which, hereafter, is considered the computational domain, is divided into a finite number of parts called “elements”. This key step is called the domain discretization. Figure 1 shows a typical grid in the aneurismal wall. Taking advantage of axisymmetry in geometry, here, nine-node quadratic rectangular plane elements are used for the domain discretization. Having discretized the computational domain, the following steps are performed.

#### a) Applying the finite-element approximations.

In order to discretize the continuous Eqs. (1) and (2), an approximate method is needed. In this work, the Galerkin’s weighted residual method is applied to the governing equations to obtain the element equations.

In the element equations, the stiffness matrix relates the amplitude of the nodal forces to that of the displacements. The shape of the finite element used in the present work is shown in Figure 2. As Figure 2 shows, there are nine nodes in each element. The radial and axial components of the displacement vector are approximated by the following equations:

$$u(z, r) = \sum_{j=1}^9 \phi_j u_j, \quad (18)$$

$$v(z, r) = \sum_{j=1}^9 \phi_j v_j, \quad (19)$$

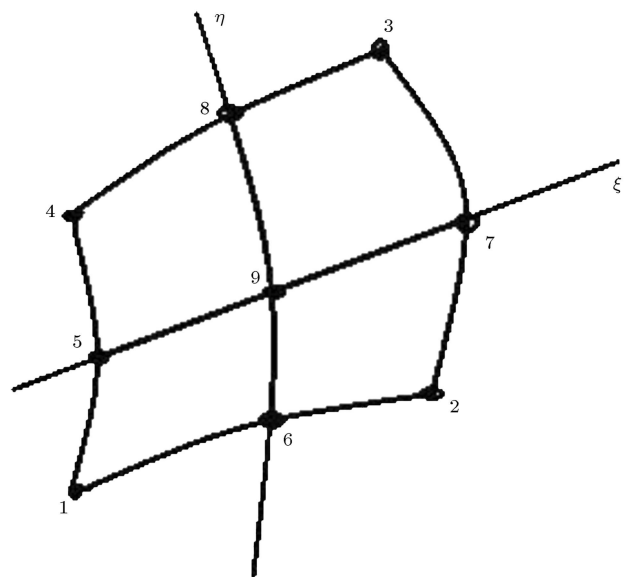


Figure 2. The nine-node finite-element.

in which,  $u$  is the axial and  $\nu$  is the radial component of the displacement vector. The shape functions,  $\phi_j$ , are defined by the following equations:

$$\phi_1 = \frac{1}{4}\xi\eta(1-\xi)(1-\eta), \quad (20)$$

$$\phi_2 = -\frac{1}{4}\xi\eta(1+\xi)(1-\eta), \quad (21)$$

$$\phi_3 = \frac{1}{4}\xi\eta(1+\xi)(1+\eta), \quad (22)$$

$$\phi_4 = -\frac{1}{4}\xi\eta(1-\xi)(1+\eta), \quad (23)$$

$$\phi_5 = -\frac{1}{2}\xi(1-\xi)(1-\eta^2), \quad (24)$$

$$\phi_6 = -\frac{1}{2}\eta(1-\xi^2)(1-\eta), \quad (25)$$

$$\phi_7 = \frac{1}{2}\xi(1+\xi)(1-\eta^2), \quad (26)$$

$$\phi_8 = \frac{1}{4}\eta(1-\xi^2)(1+\eta), \quad (27)$$

$$\phi_9 = (1-\xi^2)(1-\eta^2). \quad (28)$$

Using the shape functions as the weight functions, integration of the governing equations over the element area gives the following equations:

$$\sum_j (A_{ij}^{uu} u_j + A_{ij}^{u\nu} \nu_j) = f_{zi}, \quad (29)$$

$$\sum_j (A_{ij}^{\nu u} u_j + A_{ij}^{\nu\nu} \nu_j) = f_{ri}, \quad (30)$$

where  $f_{zi}$  and  $f_{ri}$  are nodal forces in  $z$  and  $r$  directions, respectively, and  $A$ 's are the coefficients resulting from integration of the equilibrium equations over the area of a typical element. As a typical coefficient,  $A_{ij}^{uu}$  is defined by the following equation:

$$A_{ij}^{uu} = \int_{A_e} r E_{zz} \frac{\partial \phi_i}{\partial z} \frac{\partial \phi_j}{\partial z} dA + \int_{A_e} r G_{zr} \frac{\partial \phi_i}{\partial r} \frac{\partial \phi_j}{\partial r} dA, \quad (31)$$

in this step, for each element, a system of equations is generated.

**b) Assemblage of the element equations.** At this stage, the element equations are added up to address the connection between elements in a global system. Generation of a global system of equations is the result of this step.

**c) Enforcing the boundary conditions.** Blood pressure imposed onto the inner wall, axial tension existing at the ends, and tethering stress resulting from surrounding tissues imposed onto the outer wall are considered in this step. Formulation of these boundary conditions can be summarized in the following equations:

$$\sigma_r = -P \quad \text{at} \quad r = r_i, \quad (32)$$

$$\sigma_z = \sigma_{z_o} \quad \text{at} \quad z = \pm z_m, \quad (33)$$

$$\sigma_r = -K_r \nu \quad \text{at} \quad r = r_o. \quad (34)$$

**d) Solving the system of equations in an iterative aspect due to non-linearity of the governing equations.** A band-width Gaussian-elimination method is used to solve the generated system of equations in each iteration. Details of the finite-element method can be found in any relevant textbook, such as Zienkiewics and Cheung [26], Reddy [27], Rao [28] and Comini [29]. For solving the system of nonlinear discretized governing equations, some initial values are assumed for the elastic moduli in the first iteration. After doing the first iteration and calculating the stretch ratios, the elastic moduli are modified using Eqs. (14) to (16) and calculation of the displacements is repeated until the convergence occurs.

#### 4. Validation of the method

The formulations of the problem have been implemented in a computer code to solve the generated system of equations. The computer code has been compiled and run using Lahey Fortran compiler version 5.7. First, the code has been run to check the validation of the method. To do so, a simple case, in which the thickness and radius are uniform, was considered. The numerical results have been compared with the analytical solution obtained by solving a simple differential equation and applying boundary conditions. In fact, this case is a thick-wall cylinder and has the following analytical solution:

$$\sigma_r = C_1 - \frac{C_2}{r^2}, \quad (35)$$

$$\sigma_\theta = C_1 + \frac{C_2}{r^2}, \quad (36)$$

in which:

$$C_1 = \frac{r_i^2 P [K_r r_o (1 + \nu) - E_r] E_r}{(r_i^2 - r_o^2) E_r - (1 - \nu) K_r r_o^3 - (1 + \nu) K_r r_o r_i^2}, \quad (37)$$

$$C_2 = \frac{r_i^2 r_o^2 P [K_r r_o (1 - \nu) + E_r]}{(r_i^2 - r_o^2) E_r - (1 - \nu) K_r r_o^3 - (1 + \nu) K_r r_o r_i^2}, \quad (38)$$

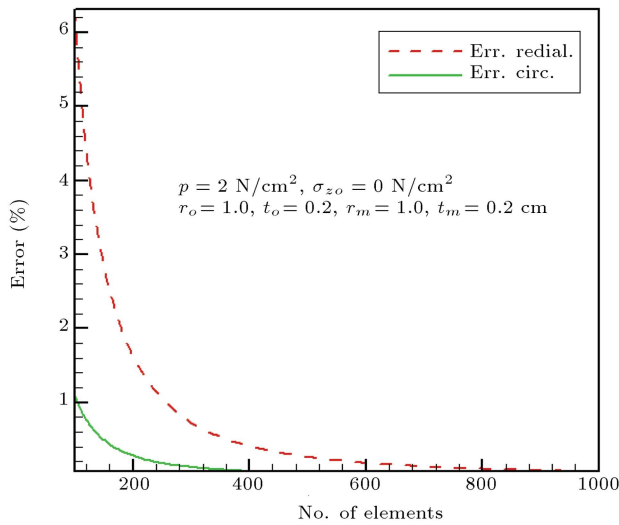


**Figure 3.** Numerical error versus number of elements.

in Eqs. (37) and (38),  $K_r$  is the tethering coefficient and it is assumed that the outer wall is acted upon by radial tethering stress. In Figure 3, the numerical results are compared with the analytical solution. Figure 3 shows that the numerical error in calculation of radial stress declines from 6.32% to about 0.06%, while the numerical error in calculation of circumferential stress decreases from 1.09% to about 0.01, as the number of elements increases from 100 to 1000. The percentage of relative errors, shown in Figure 3, was calculated according to the following formula:

$$\% \text{Err.} = \frac{|\sigma_{\text{Ana.}} - \sigma_{\text{Num.}}|}{\sigma_{\text{Ana.}}} \quad (39)$$

## 5. Results

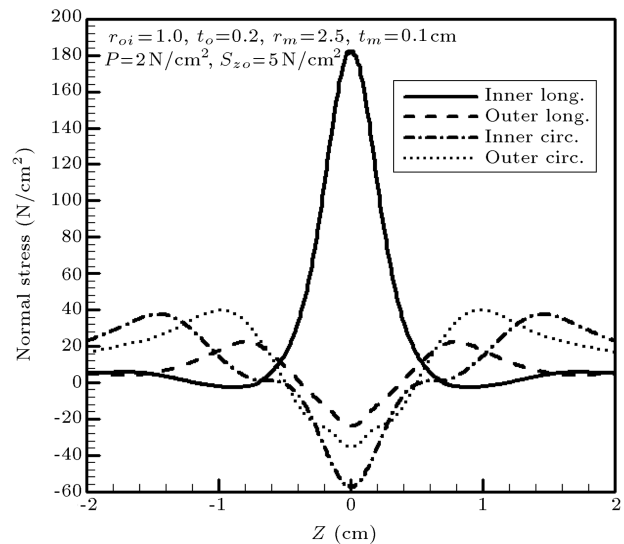
After validation of the method, the effects of factors such as aneurysm radius, blood pressure, central aneurysmal wall thickness and longitudinal tension on stress distribution in the aneurysmal wall have been studied for both uniform and non-uniform stiffness.

The longitudinal and circumferential stress distributions on the inner and outer surfaces for a typical case are plotted in Figure 4. It is necessary to point out that the thick-wall theory calculates the stress distribution along the aneurysm length as well as across the wall thickness, while simpler methods, such as the membrane theory, calculate the stress distribution only along the aneurysm length, by considering a meridional line in the middle of the thickness. In this figure, the inner and outer stresses are compared. Figure 4 implies that the stress varies significantly across the wall thickness. This figure indicates that the maximum longitudinal stress occurs at the aneurysm center on the inner surface, while on the outer surface, the longitudinal stress is negative, i.e. compressive at this section. Therefore, the simpler methods reduce this

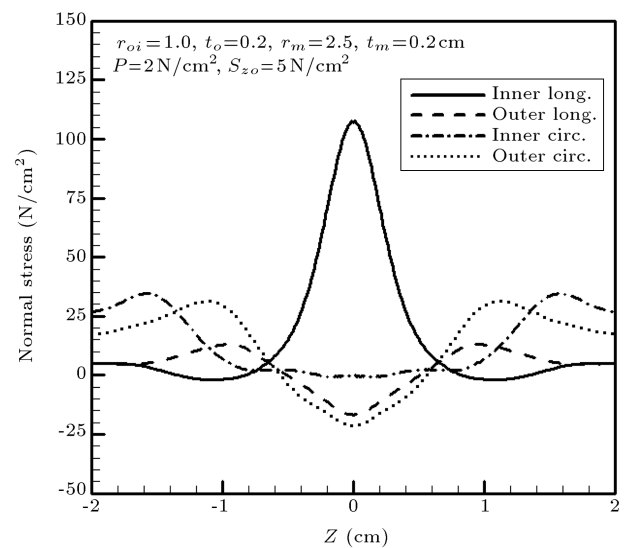
stress in this cross section by averaging across the thickness.

Figure 4 also indicates that the cross section of maximum circumferential stress on the inner surface differs from that on the outer surface. Therefore, the simpler methods reduce the predicted maximum circumferential stress by averaging across the thickness. The location of the maximum longitudinal stress is on the aneurysm center and occurs on the inner surface, while the location of the maximum circumferential stress is in the vicinity of the aneurysm center and occurs both on the inner and outer surfaces at different locations. This difference is not only for non-uniform thickness but also for uniform thickness.

Figure 5 portrays the same results for  $t_m =$



**Figure 4.** Stress distribution along the aneurysm length for  $t_m = 0.1$  cm.



**Figure 5.** Stress distribution along the aneurysm length for  $t_m = 0.2$  cm.

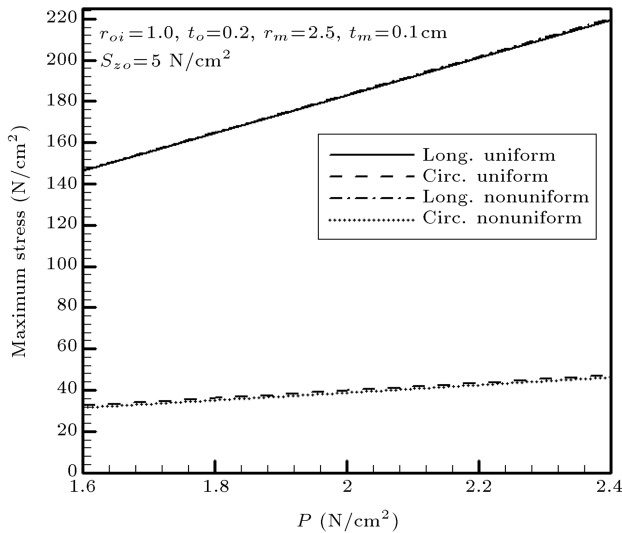


**Figure 6.** Maximum longitudinal and circumferential stresses versus blood pressure for uniform and non-uniform stiffness.

0.2 cm, which is equal to the (i.e. thickness ratio equal to 1), while Figure 4 is plotted for  $t_m/t_o = 0.5$  (i.e. thickness ratio equal to 0.5). Therefore, regardless of the aneurysm wall thickness ratio, maximum longitudinal stress occurs in the aneurysm center and maximum circumferential stress occurs in the vicinity of the aneurysm center. In addition, Figures 4 and 5 show that maximum circumferential stress is less than maximum longitudinal stress for this range of thickness ratio.

Figure 6 shows the variation of maximum longitudinal and circumferential stresses versus blood pressure for both uniform and non-uniform stiffness. This figure indicates that there is no significant difference between uniform and non-uniform stiffness. In addition, the maximum longitudinal stresses increases linearly from  $146 \text{ N/cm}^2$  to about  $220 \text{ N/cm}^2$  as the blood pressure increases from  $1.6 \text{ N/cm}^2$  ( $120 \text{ mmHg}$ ) to  $2.4 \text{ N/cm}^2$  ( $180 \text{ mmHg}$ ). This is despite the fact that the constitutive relation is non-linear. This result might be due to the fact that the stress does not depend on the elastic modulus in simple cases. For example, in simple tension, the stress equals the ratio of the force to the sectional area and does not depend on the elastic modulus.

Figures 7, 8 and 9 show the variation of maximum longitudinal and circumferential stresses versus aneurysm radius, aneurysm wall thickness and axial tension, respectively, for both uniform and non-uniform stiffness. These figures also indicate that there is no significant difference between uniform and non-uniform stiffness, except for high axial tension that may not occur in practical cases.

Figure 7 demonstrates that maximum longitudinal stress increases from  $12 \text{ N/cm}^2$  to about

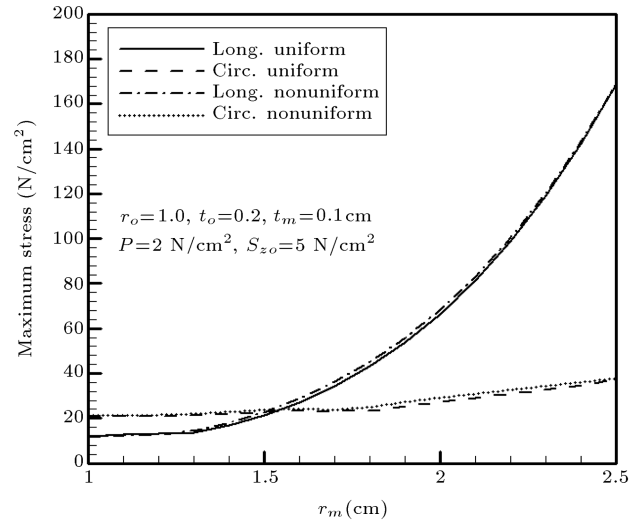


**Figure 7.** Maximum longitudinal and circumferential stresses versus aneurysm radius for uniform and non-uniform stiffness.

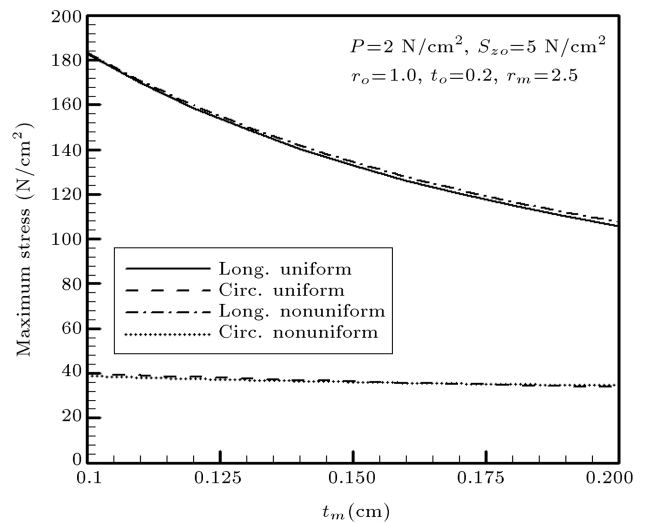


**Figure 8.** Maximum longitudinal and circumferential stresses versus aneurysm wall thickness for uniform and non-uniform stiffness.

$168 \text{ N/cm}^2$ , while maximum circumferential stress increases from  $21 \text{ N/cm}^2$  to about  $37 \text{ N/cm}^2$  as the aneurysm radius increases from  $1.0 \text{ cm}$  to  $2.5 \text{ cm}$ .

Figure 8 shows that maximum longitudinal stress declines from  $183 \text{ N/cm}^2$  to about  $106 \text{ N/cm}^2$ , while maximum circumferential stress decreases from  $40 \text{ N/cm}^2$  to about  $35 \text{ N/cm}^2$  as the aneurysm wall thickness increases from  $0.1 \text{ cm}$  to  $0.2 \text{ cm}$ .

Figure 9 indicates that maximum longitudinal stress rises from  $177 \text{ N/cm}^2$  to about  $218 \text{ N/cm}^2$ , while maximum circumferential stress increases from  $40 \text{ N/cm}^2$  to about  $78 \text{ N/cm}^2$  according to non-uniform stiffness and  $49 \text{ N/cm}^2$  according to uniform stiffness, as the aneurysm axial tension increases from  $4 \text{ N/cm}^2$  to about  $12 \text{ N/cm}^2$ .

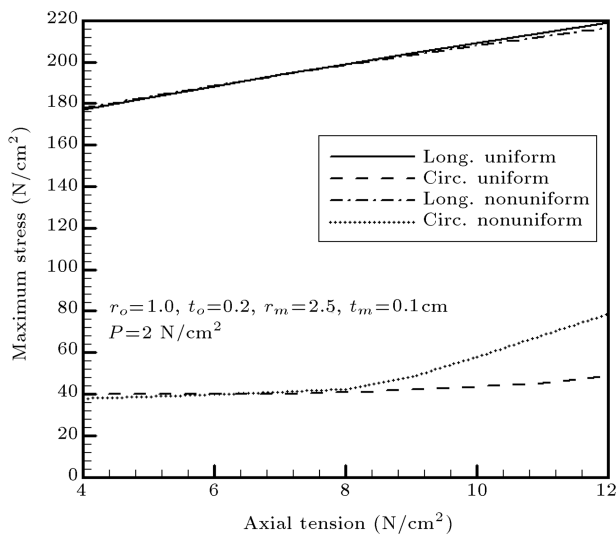


**Figure 9.** Maximum longitudinal and circumferential stresses versus axial tension for uniform and non-uniform stiffness.

## 6. Conclusions

In this study, the thick-wall theory is used to find the effect of non-uniform stiffness on stress distribution and maximum stress generated in the aneurysm wall. The full equilibrium equations are solved by the FEM with nine-node quadratic rectangular plane elements. The results of the present work demonstrate that stress distribution and, consequently, maximum stress are not only affected by aneurysm size, but are also significantly affected by factors such as arterial wall thickness and blood pressure, as well as longitudinal tension. Stress distribution is not significantly affected by the uniformity or non-uniformity of the wall stiffness. The results obtained from this study show that the maximum stress generated in the wall is longitudinal stress and occurs on the inner surface. In such cases, maximum longitudinal stress on the inner surface is much more than that on the outer surface.

## Nomenclature

$E$	Elastic modulus
$E_0$	Elastic modulus at the aneurysm center
$P$	Blood pressure
$\sigma_z$	Longitudinal stress
$\sigma_\theta$	Circumferential stress
$r$	Radial coordinate
$r_o$	Inner radius at the inlet section
$r_m$	Inner radius at the aneurysm center
$t_o$	Wall thickness at the inlet section
$t_m$	Wall thickness at the aneurysm center
$z$	Longitudinal coordinate

## References

- Judd, S.J., *Blood and Circulatory Disorders*, Detroit, Health Reference Series, Omnigraphics, Inc. (2010).
- Katz, D.A., Littenberg, B. and Cronenwett, J.L. "Management of small abdominal aortic aneurysms: Early surgery to watchful waiting", *JAMA*, **268**, pp. 2678-2686 (1992).
- Ezekowics, M.D., *Systematic Cardiac Embolism*, New York, Marcel Dekker (1993).
- Raghavan, M.L. and Vorp, D.A. "Toward a biomechanical tool to evaluate rupture potential of abdominal aortic aneurysm: Identification of a finite strain constitutive model and evaluation of its applicability", *Journal of Biomechanics*, **33**, pp. 475-482 (2000).
- Fillinger, M. "The long-term relationship of wall stress to the natural history of AAA", *Annals of the New York Academy of Sciences*, **1085**, pp. 22-28 (2006).
- Vorp, D.A., Schiro, B.J., Ehrlich, M.P., Juvonen, T.S., Ergin, M.A. and Griffith, B.P. "Effect of aneurysm on the tensile strength and biomechanical behavior of the ascending thoracic aorta", *Annular Thoracic Surgery*, **75**, pp. 1210-1214 (2003).
- Inzoli, F., Boschetti, F., Zappa, M., Longo, T. and Fumero, R. "Biomechanical factors in abdominal aortic aneurysm rupture", *European Journal of Vascular Surgery*, **7**, pp. 667-674 (1993).
- Mower, W.R., Baraff, L.J. and Sneyd, J. "Stress distributions in vascular aneurysms: factors affecting risk of aneurysm rupture", *Journal of Surgical Research*, **55**, pp. 155-161 (1993).
- Stringfellow, M.M., Lawrence, P.F. and Stringfellow, R.G. "The influence of aorta-aneurysm geometry upon stress in the aneurysm wall", *Journal of Surgical Research*, **42**, pp. 425-433 (1987).
- Elger, D.F., Blacketter, D.M., Budwig, R.S. and Johansen, K.H. "The influence of shape on the stresses in model abdominal aortic aneurysms", *Journal of Biomechanical Engineering*, **118**, pp. 326-332 (1996).
- Vorp, D.A., Raghavan, M.L. and Webster, M.W. "Stress distribution in abdominal aortic aneurysm: Influence of diameter and asymmetry", *Journal of Vascular Surgery*, **27**, pp. 632-639 (1998).
- Hung, E.J.N. and Botwin, M.R. "Mechanics of rupture of cerebral saccular aneurysms", *Journal of Biomechanics*, **8**, pp. 385-392 (1975).
- Geest, J.P.V., Sacksa, M.S. and Vorp, D.A. "The effects of aneurysm on the bilongitudinal mechanical behavior of human abdominal aorta", *Journal of Biomechanics*, **39**(7), pp. 1324-1334 (2006).
- Steiger, H.J., Aaslid, R., Keller, S. and Reulen, H.J. "Strength, elasticity and viscoelastic properties of cerebral aneurysms", *Heart and Vessels*, **5**(1), pp. 41-46 (1989).
- Demiray, H. "A quasi-linear constitutive relation for arterial wall material", *Journal of Biomechanics*, **29**(8), pp. 1011-1014 (1996).

16. Kyriacou, S.K. and Humphrey, J.D. “Influence of size, shape and properties on the mechanics of axisymmetric saccular aneurysms”, *Journal of Biomechanics*, **29**(8), pp. 1015-1022 (1996).
17. Shah, A.D. and Humphrey, J.D. “Finite strain elastodynamics of intracranial saccular aneurysms”, *Journal of Biomechanics*, **32**, pp. 593-599 (1999).
18. Hademenos, G.L., Massoud, T., Valentino, D.J., Duckwiler, G. and Vinuela, F.A. “Nonlinear mathematical model for the development and rupture of intracranial fusiform aneurysms”, *Neurol Research*, **16**(6), pp. 433-438 (1994).
19. Thubrikar, M.J., Agali, P. and Robicsek, F. “Wall stress as a possible mechanism for the development of transverse intimal tears in aortic dissections”, *Journal of Medical Engineering and Technology*, **23**(4), pp. 127-134 (1999).
20. Merckx, M.A.G., Veer, M., Speelman, L., Breeuwer, M., Buth, J. and Vosse, F.N. “Importance of initial stress for abdominal aortic aneurysm wall motion: Dynamic MRI validated finite element analysis”, *Journal of Biomechanics*, **42**(14), pp. 2369-2373 (2009).
21. Gasser, T.C. “An irreversible constitutive model for fibrous soft biological tissue: A 3-D microfiber approach with demonstrative application to abdominal aortic aneurysms”, *Acta Biomaterialia*, **7**(6), pp. 2457-2466 (2011).
22. Gasser, T.C., Gallinetti, S., Xing, X., Forsell, C., Swedenborg, J. and Roy, J. “Spatial orientation of collagen fibers in the abdominal aortic aneurysm’s wall and its relation to wall mechanics”, *Acta Biomaterialia*, **8**(8), pp. 3091-3103 (2012).
23. Polzer, S., Gasser, T.C., Bursa, J., Staffa, R., Vlachovsky, R., Man, V. and Skacel, P. “Importance of material model in wall stress prediction in abdominal aortic aneurysms”, *Medical Engineering & Physics*, **35**(9), pp. 1282-1289 (2013).
24. Timoshenko, S. and Goodier, J.N., *Theory of Elasticity*, McGraw-Hill (1997).
25. Atkin, R.J. and Fox, N., *An Introduction to the Theory of Elasticity*, Dover Publications (2005).
26. Zienkiewicz, O.C. and Cheung, Y.K., *The Finite Element Method in Structural and Continuum Mechanics*, McGraw-Hill (2000).
27. Reddy, J.N., *An Introduction to the Finite Element Method*, McGraw-Hill (2000).
28. Rao, S.S., *The Finite Element Methods in Engineering*, Butterworth Heinemann (1999).
29. Comini, G., *Finite Element Analysis in Heat Transfer: Basic Formulation and Linear Problems*, Taylor & Francis (1994).

### Biography

**Gholam Reza Zendehebudi** received BS, MS and PhD degrees in Mechanical Engineering from Shiraz University, Iran, in 1987, 1990 and 1999, respectively. He is currently Assistant Professor in the Department of Mechanical Engineering at Yasouj University, Iran, where he teaches courses in his field of expertise, including advanced mathematics, gas dynamics, heat transfer and fluid mechanics. His research interests include CFD, heat transfer, biomechanics, and the application of the finite element method in fluid flow and free convection. His papers have been published in a number of high quality journals.